Global Biogeochemical Cycles

Supporting Information for

Assessment of Global Ocean Biogeochemistry Models for Ocean Carbon Sink Estimates in RECCAP2 and Recommendations for Future Studies

Jens Terhaar[1,2,3,†], Nadine Goris[4,†], Jens D. Müller[5], Tim DeVries[6,7], Nicolas Gruber[5], Judith Hauck[8], Fiz F. Perez[9], Roland Séférian[10]

[1]Department of Marine Chemistry and Geochemistry, Woods Hole Oceanographic Institution, Woods Hole, 02543, Massachusetts, USA

[2]Climate and Environmental Physics, Physics Institute, University of Bern, Switzerland

[3]Oeschger Centre for Climate Change Research, University of Bern, Switzerland

[4]NORCE Climate & Environment, Bjerknes Centre for Climate Research, Bergen, Norway

[5]Environmental Physics, Institute of Biogeochemistry and Pollutant Dynamics, ETH Zurich, Zürich, Switzerland

[6]Department of Geography, University of California, Santa Barbara, Santa Barbara, CA, USA

[7]Earth Research Institute, University of California, Santa Barbara, Santa Barbara, CA, USA

[8]Alfred-Wegener-Institut, Helmholtz-Zentrum für Polar- und Meeresforschung, Am Handelshafen 12, 27570 Bremerhaven, Germany

[9]Instituto de Investigaciones Marinas (IIM), CSIC, Vigo, Spain. (0000-0003-4836-8974)

[10]CNRM (Université de Toulouse, Météo-France, CNRS), Toulouse, France]

Contents of this file

Text S1.

The GOBM PlankTOM12 is not considered in this study for anthropogenic flux and storage analysis as Planktom12 simulates almost no accumulation of C_{ant} in the high latitude North Atlantic but a large accumulation in the high-latitude North Pacific, where neither the other GOBMs nor the observation-based estimate from GLODAPv2 indicate an accumulation of C_{ant}. This anomalous pattern is driven by a strong negative upper ocean (0-150 m) salinity bias in the North Atlantic and a positive salinity bias in the North Pacific. These biases in the salinity cause upper ocean density biases (Figures S9 and S10), which cause the overly strong accumulation of C_{ant} in the North Pacific and the overly weak Cant accumulation in the North Atlantic. The salinity-density bias also extends in the surface Southern Ocean, where the inter-frontal sea surface density of PlanktTOM12 is the lowest density among all GOBMs (1026.91 kg m^{-3}). The salinity bias decreases over the time of the simulation period (1980 to 2018) to almost zero. The size and the temporal evolution of the bias suggests that the model has been far away from equilibrium at the start of the analyzing period, possibly due to a change in the external forcing or other model set-up changes.

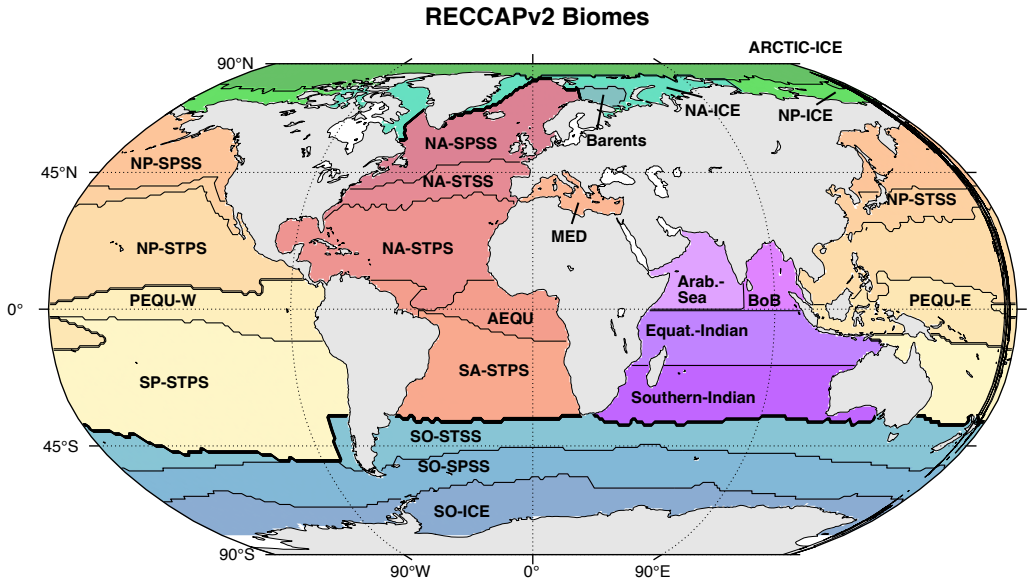

Figure S1. Biome-mask as utilized in RECCAP2 and within this study. The shading of the biomes is based on the ocean basin considered (Atlantic: orange-red, Pacific: yellow-orange, Southern Ocean: shades of blue, Indian Ocean: shades of lilac, Arctic: shades of green). In most cases, the letters before the hyphen denote the geographical location of the biome (NA: North Atlantic, SA: South Atlantic, AEQ: Atlantic equator, NP: North Pacific, SP: South Pacific, PEQ: Pacific Equator, SO: Southern Ocean) and the following letters describe their characteristics (SPSS: subpolar and seasonally stratified, STSS: subtropical and seasonally stratified, STPS: subtropical and permanently stratified, ICE: marginal sea-ice and U: upwelling). The Pacific equatorial upwelling biome is divided in east (E) and west (W). The newly introduced biomes here only describe the ocean region by name and are mostly self-explanatory with two exceptions (MED: Mediterranean Sea, BoB: Bay of Bengal).

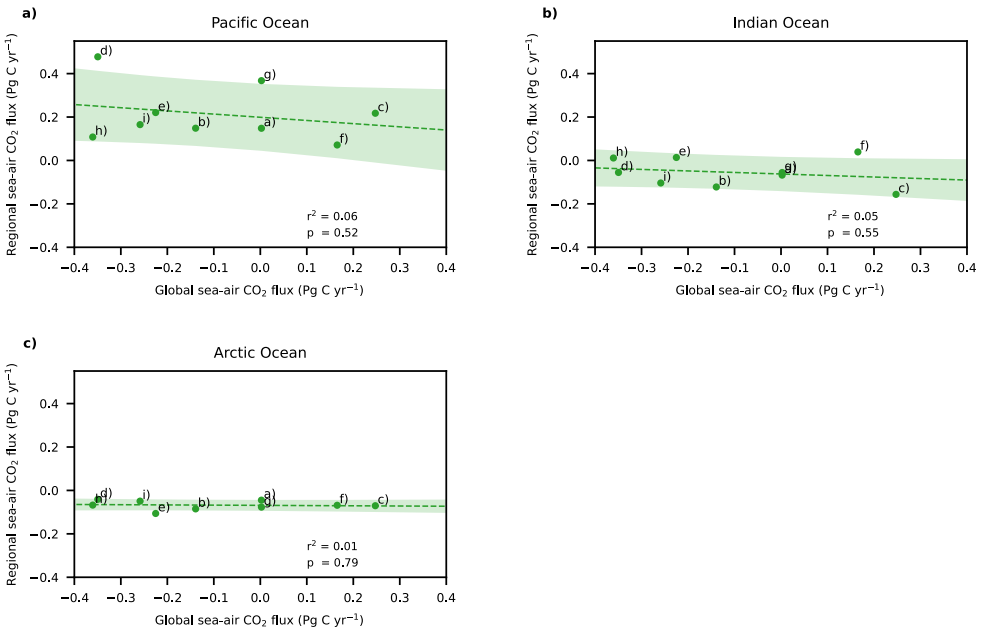

Figure S2. Regional ocean sea-air CO_2 fluxes against global sea-air CO2 flux in simulation B for 10 GOBMs. For each GOBM the regional sea-air CO_2 flux in simulation B in the a) Pacific, b) Indian, and c) Arctic Ocean, representing the natural sea-air CO_2 flux plus a potential sea-air CO_2 flux due to an interior ocean drift or carbon fluxes from rivers and into sediments is plotted against the global ocean sea-air CO_2 flux in simulation B. The dashed line indicates a linear fit and the shading the projection uncertainty with a 68% uncertainty interval.

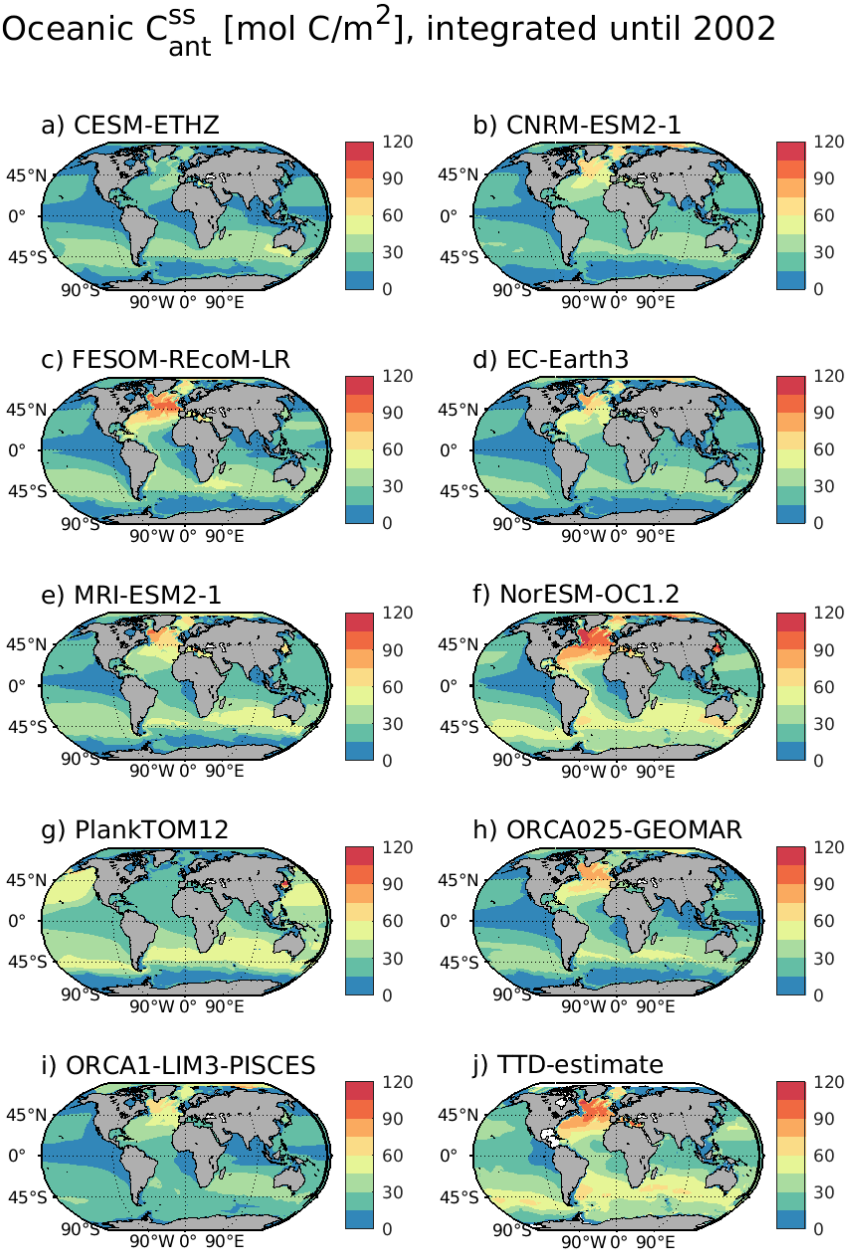

Figure S3: Estimated integrated anthropogenic carbon storage (steady state) from surface to 3000m depth and from initial year until 2002 for each of the considered models as well as the TTD-based estimate from GLODAPv2.2. GLODAPv2.2 assumes a pre-industrial atmospheric CO2 mixing ratio of 280 ppm, while the pre-industrial atmospheric CO2 mixing ratio varies between 278 and 287.4 for GOBMs (see Section 2.2.3).

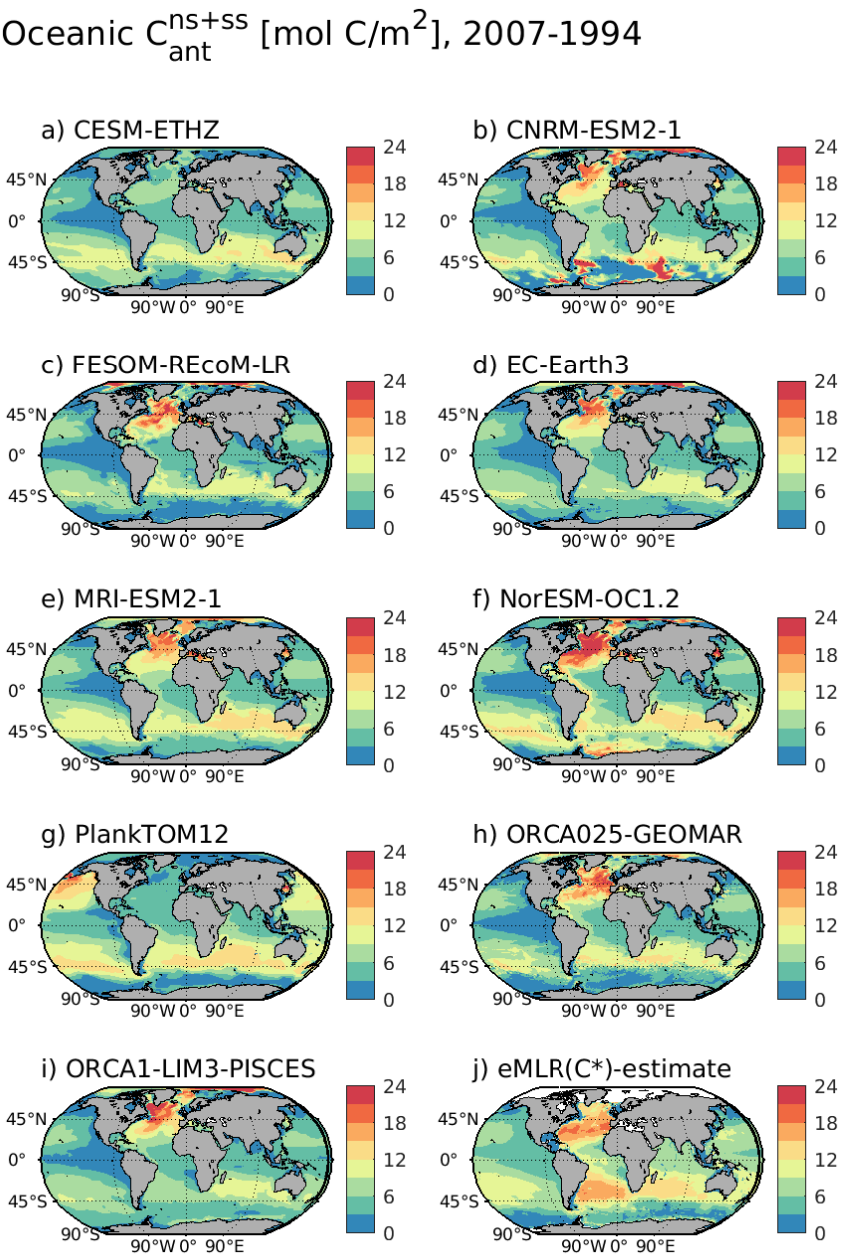

Figure S4: Estimated integrated anthropogenic carbon storage from 1994 to 2007 (non-steady and steady state), integrated from surface to 3000 m. Panels a)-i) show the estimate for each of the considered models, while panel j) shows the observation-based estimate derived with the eMLR(C*)-method (Gruber et al., 2009).

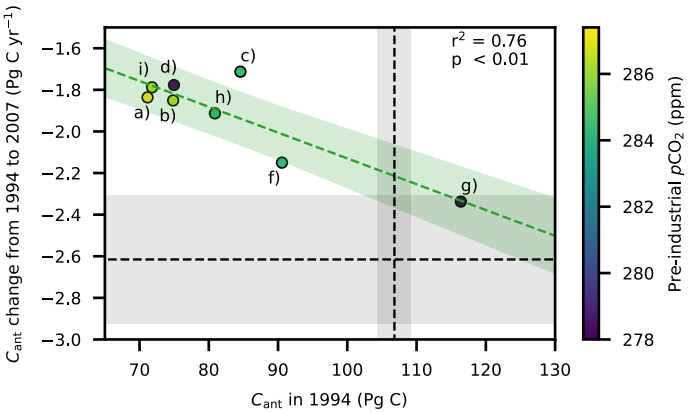

Figure S5. Relationship between long-term and recent change in marine anthropogenic carbon. Anthropogenic carbon (C_{ant}) change from pre-industrial times until 1994 compared to the change from 1994 to 2007. Colored dots show results from GOBMs and the colors show atmospheric pCO2 in the pre-industrial control simulations. The dashed green line indicates the linear fit across the GOBM ensemble, and the green shading shows the 68% projection uncertainties. Observation-based estimates from Sabine et al. (2004) for C_{ant} in 1994 and from Gruber et al. (2019) for the change in C_{ant} from 1994 to 2007 and their respective uncertainties are shown as dashed black lines and black shading.

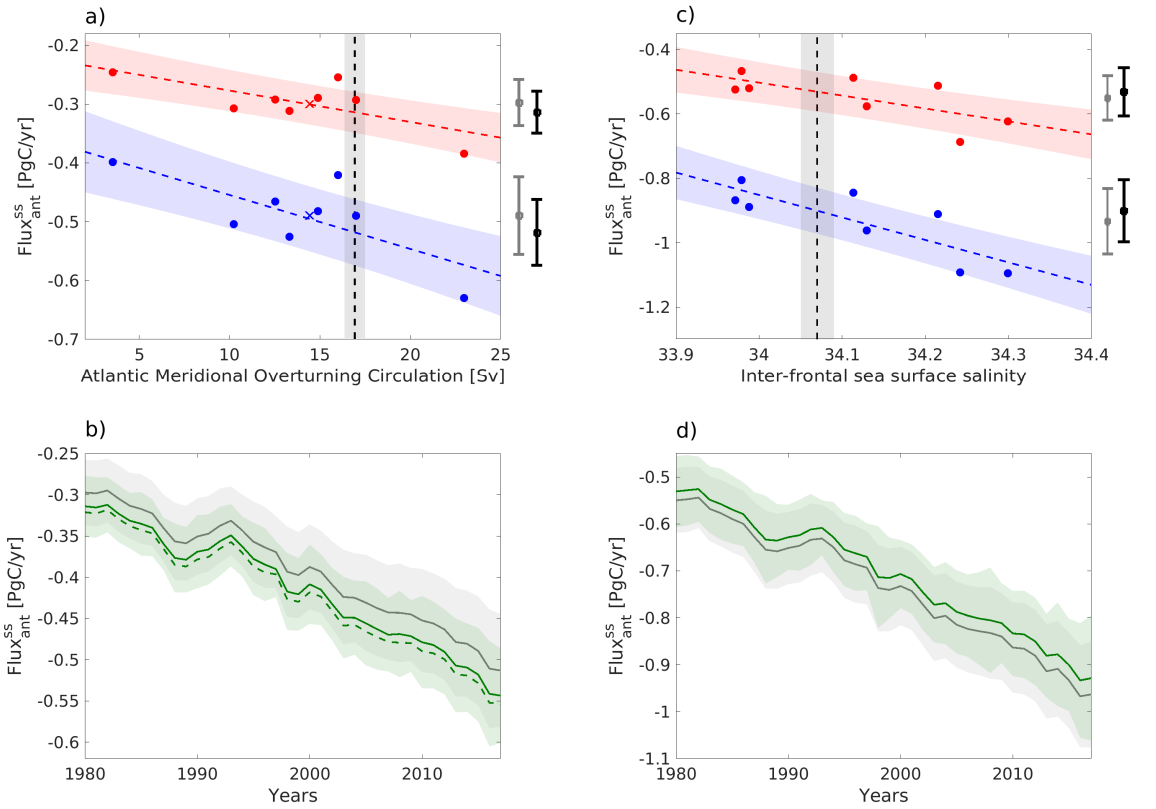

Figure S6. Temporal evolution of the constrained steady-state anthropogenic carbon uptake in the Atlantic and Southern Ocean. Emergent constraints between the simulated steady-state anthropogenic carbon uptake for the year 1980 (red dots) and 2015 (blue dots) of a) the Atlantic and c) the Southern Ocean, plotted against a) the Atlantic Meridional Overturning Circulation at 26°N averaged from 2005 to 2018, b) the inter-frontal sea surface salinity averaged from 1980 to 2018. Included are linear fits (red/blue dashed lines) with 68% projection intervals (red/blue shaded area) across GOBMs (red/blue dots) as well as observational estimates and their uncertainties (dashed black lines and black shaded area). The crosses in a) indicate an additional simulation with CESM-ETHZ (see Section 2.1 of the main article). Panels b) and d) illustrate the temporal evolution of the steady-state anthropogenic carbon uptake in b) Atlantic and d) Southern Ocean, featuring both the unconstrained estimate (gray line and gray shaded area) as well as the constrained estimate and its uncertainty (green line and green shaded area) when constraining each annual value individually using b) the Atlantic Meridional Overturning Circulation at 26°N averaged from 2005 to 2018, and d) the inter-frontal sea surface salinity averaged from 1980 to 2018. The dashed green line in b) illustrates the mean constrained estimate when using the Cant storage below 1000m as observational constraint.

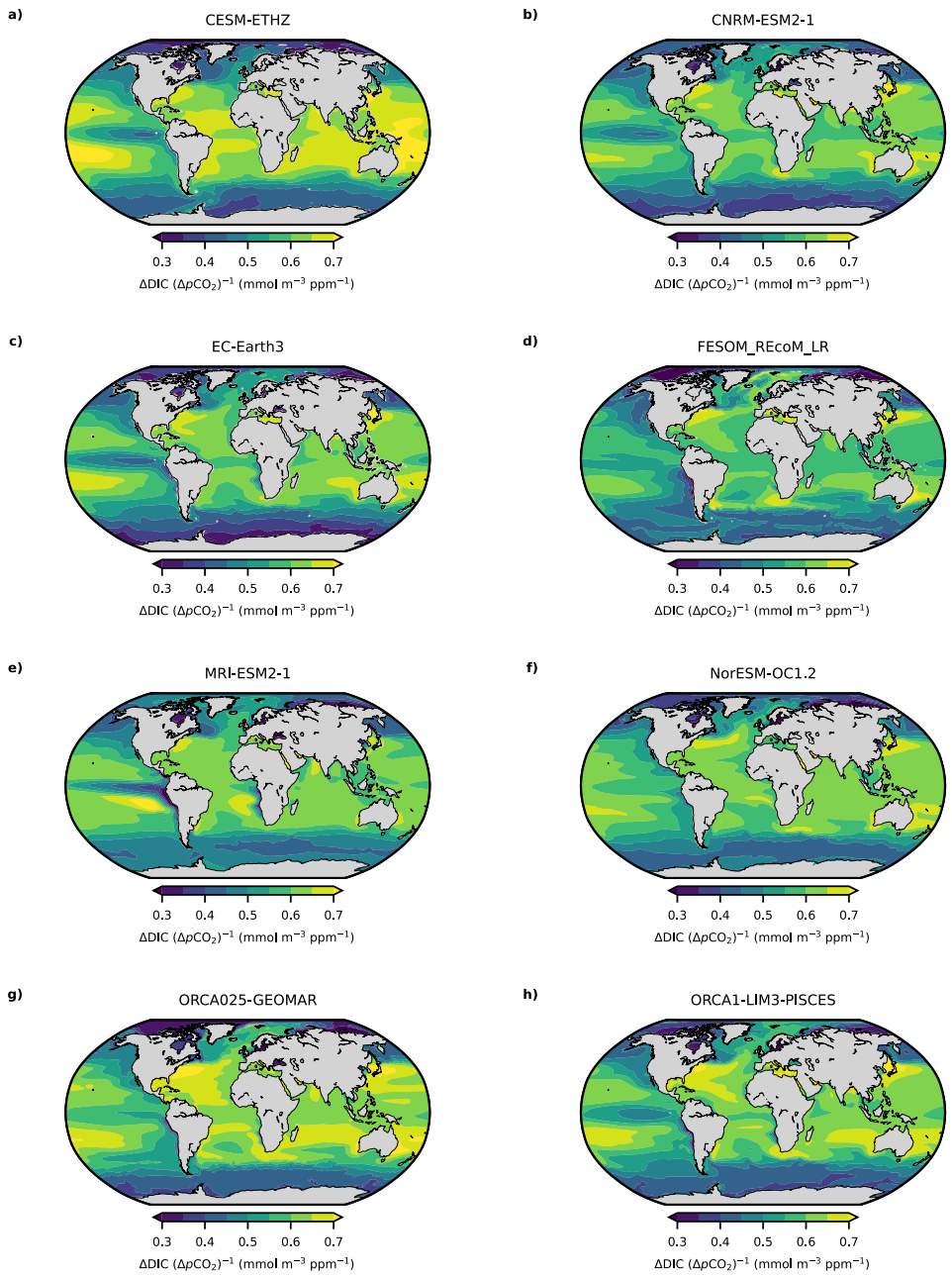

Figure S7. Surface ocean chemical uptake capacity in individual GOBMs normalized to 2002. Maps of the average increase in DIC per increase in pCO_2 averaged from 1982 to 2018 based as simulated by a) CESM-ETHZ, b) CNRM-ESM2-1, c) EC-Earth3, d) FESOM REcoM LR, e) MRI-ESM2-1, f) NorESM-OC1.2, g) ORCA025-GEOMAR, and h) ORCA1-LIM3-PISCES.

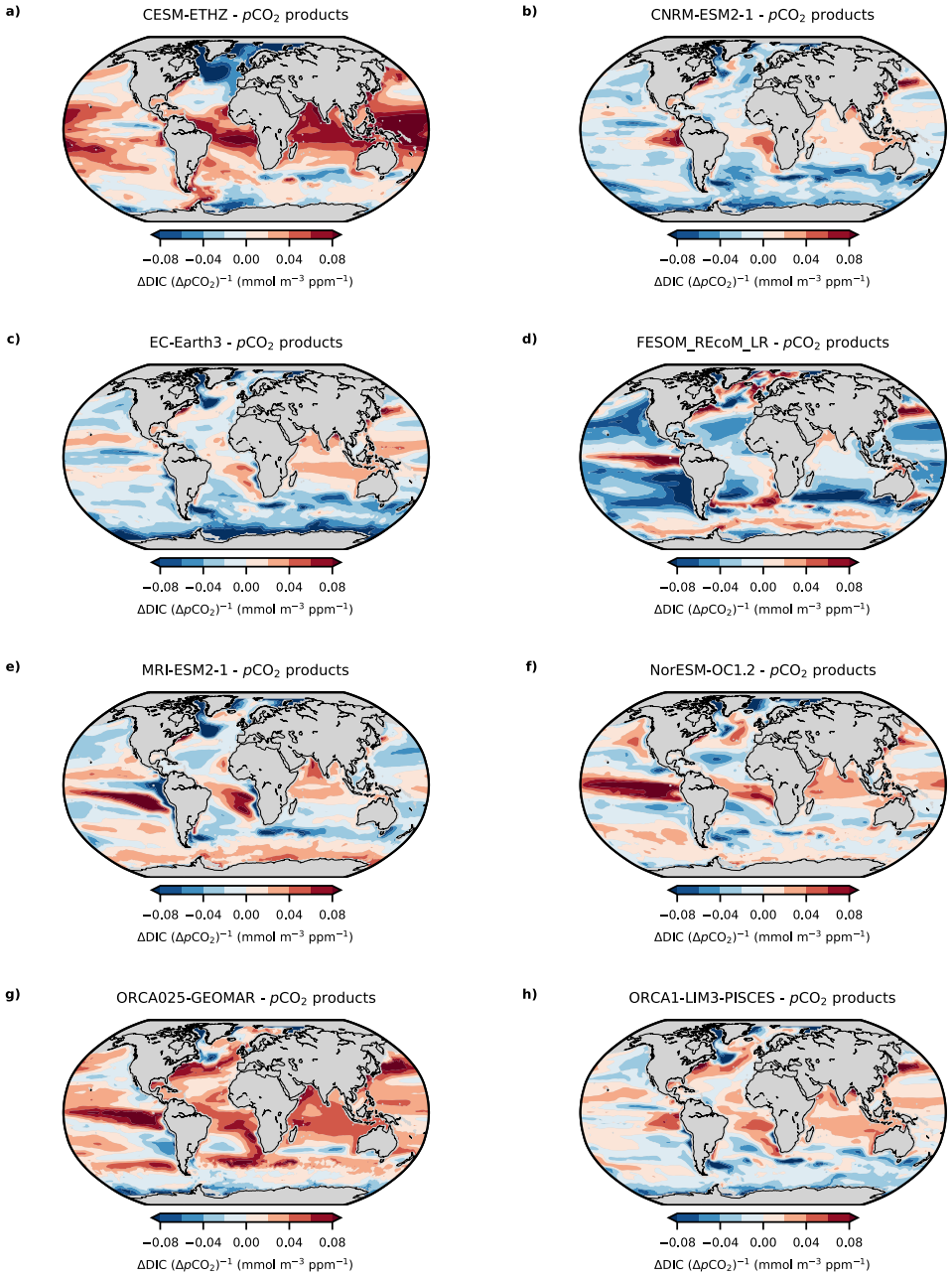

Figure S8. Difference between surface ocean chemical uptake capacity normalized to 2002 in individual GOBMs and pCO_2/alkalinity products. Maps of the difference in average increase in DIC per increase in pCO_2 averaged from 1982 to 2018 based as simulated by a) CESM-ETHZ, b) CNRM-ESM2-1, c) EC-Earth3, d) FESOM REcoM LR, e) MRI-ESM2-1, f) NorESM-OC1.2, g) ORCA025-GEOMAR, and h) ORCA1-LIM3-PISCES compared to the average of pCO_2/alkalinity products.

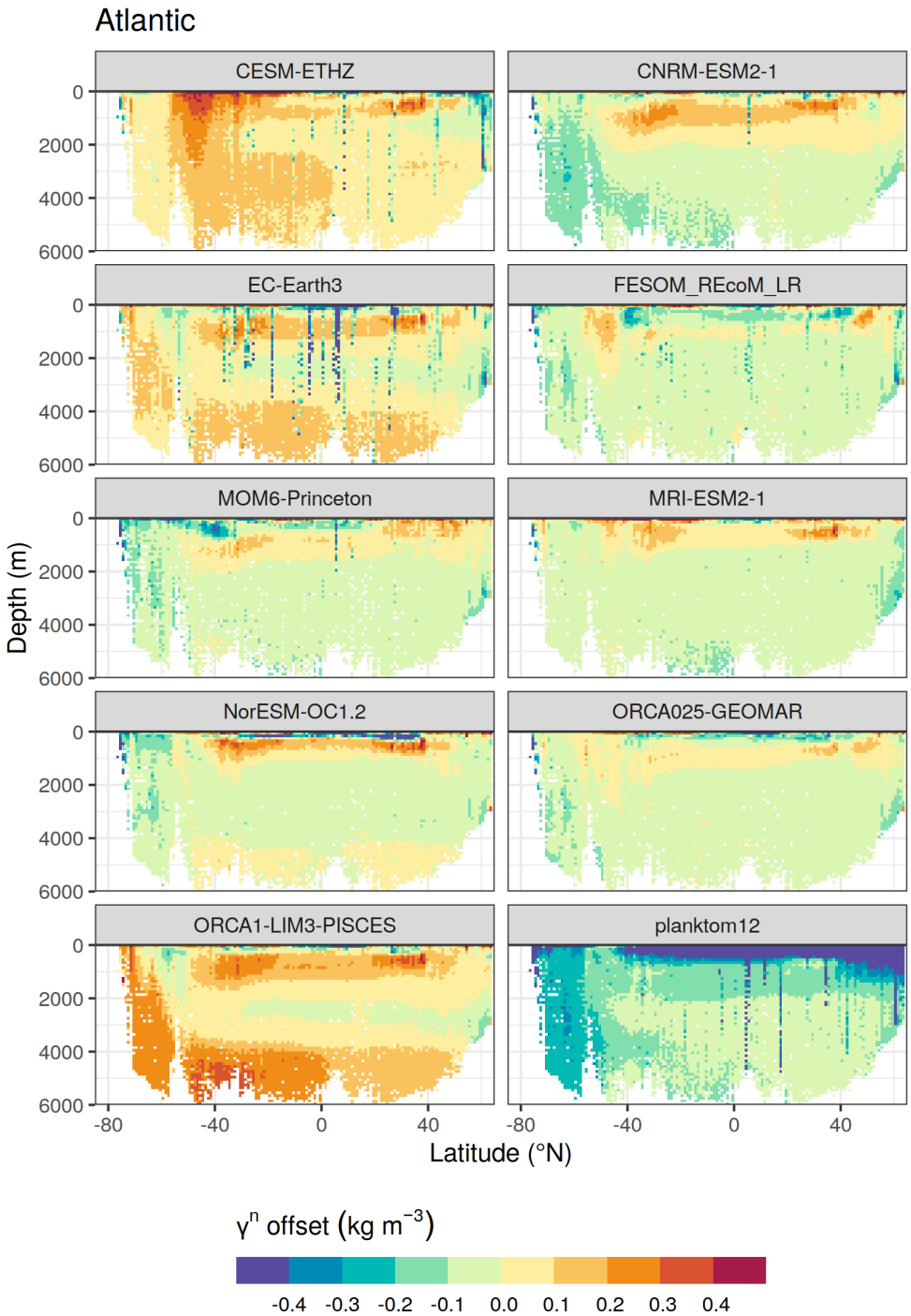

Figure S9: Neutral density zonal mean section for the Atlantic Ocean. Differences between individual GOBMs and estimates calculated from observations provided through GLODAPv2.2021 (Lauvset et al., 2021). GOBM and GLODAP data were merged on the 1°x1° horizontal grid of the models, and GOBM data were linearly interpolated in the vertical dimension to match the exact sampling depth of the observations. The zonal mean sections do not account for biases in the spatio-temporal distribution of observations.

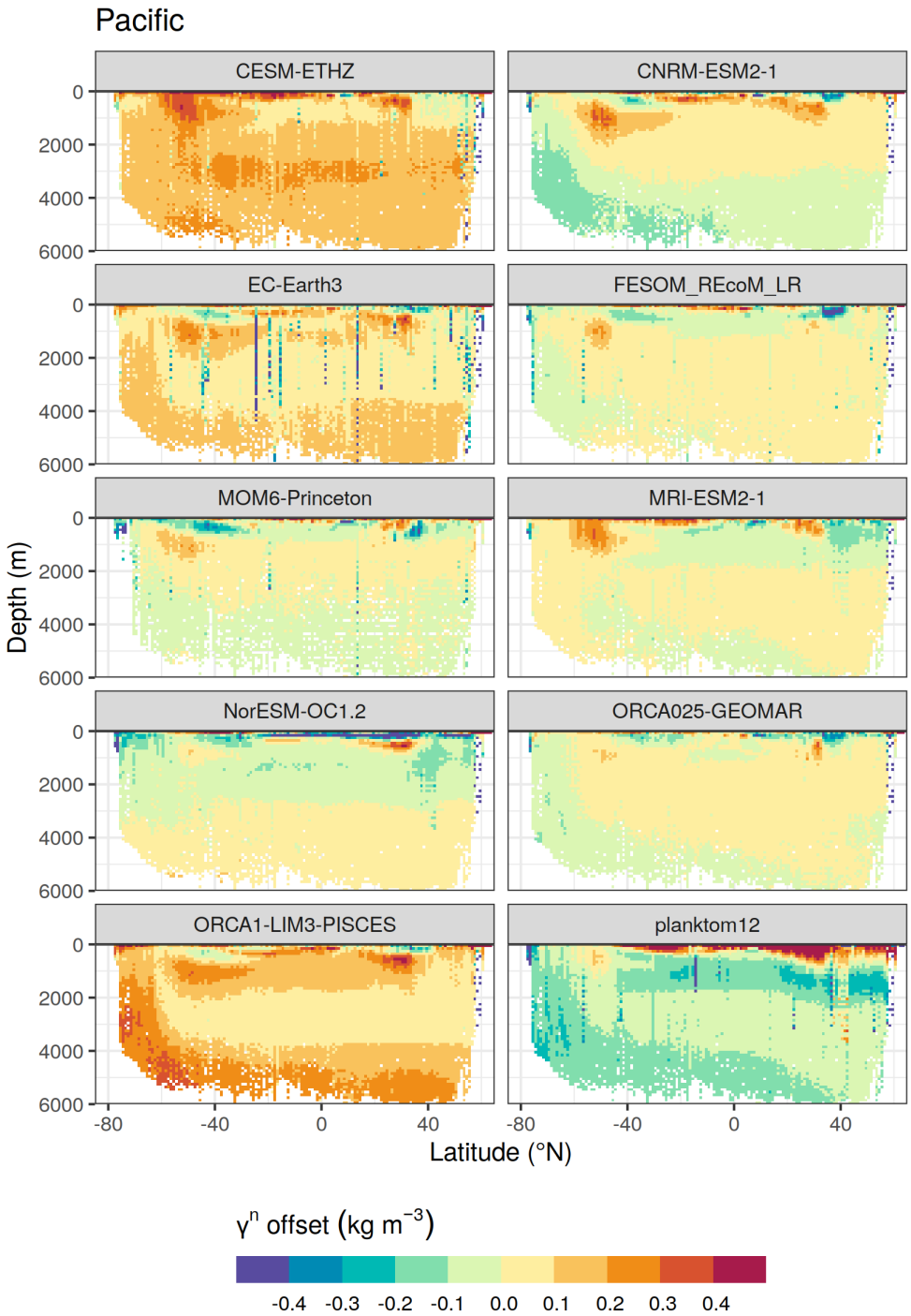

Figure S10: Neutral density zonal mean section for the Pacific Ocean. Differences between individual GOBMs and estimates calculated from observations provided through GLODAPv2.2021 (Lauvset et al., 2021). GOBM and GLODAP data were merged on the 1°x1° horizontal grid of the models, and GOBM data were linearly interpolated in the vertical dimension to match the exact sampling depth of the observations. The zonal mean sections do not account for biases in the spatio-temporal distribution of observations.

Table S1. Averaged annual standard deviations across the entire model ensemble per flux component and ocean basin. Units are in Pg C yr^{-1}.

Region	F^{total}	F^{ant}_{ss}	F^{ant}_{ns}	$F^{nat}_{ss} + F_{nat}^{riv\text{-}bur} + F^{drift+bias}$	F^{nat}_{ns}
Global Ocean	0.24	0.21	0.04	/	0.11
Atlantic Ocean	0.14	0.06	0.01	0.13	0.02
Pacific Ocean	0.15	0.08	0.02	0.14	0.09
Indian Ocean	0.08	0.03	0.01	0.06	0.03
Arctic Ocean	0.03	0.00	0.00	0.02	0.02
Southern Ocean	0.29	0.09	0.03	0.26	0.09